LANGMUIR Article
Cite This: Langmuir 2019, 35, 6971−6980
pubs.acs.org/Langmuir

Extreme Levitation of Colloidal Particles in Response to Oscillatory Electric Fields

Scott C. Bukosky,[†,‡,§] S. M. H. Hashemi Amrei,[†,§] Sean P. Rader,[†] Jeronimo Mora,[†] Gregory H. Miller,[*,†] and William D. Ristenpart[*,†]

[†]Department of Chemical Engineering, University of California Davis, Davis, California 95616, United States
[‡]Lawrence Livermore National Laboratory, Livermore, California 94551 United States

Supporting Information

ABSTRACT: Micron-scale colloidal particles suspended in electrolyte solutions have been shown to exhibit a distinct bifurcation in their average height above the electrode in response to oscillatory electric fields. Recent work by Hashemi Amrei et al. (*Phys. Rev. Lett.*, **2018**, *121*, 185504) revealed that a steady, long-range asymmetric rectified electric field (AREF) is formed when an oscillatory potential is applied to an electrolyte with unequal ionic mobilities. In this work, we use confocal microscopy to test the hypothesis that a force balance between gravity and an AREF-induced electrophoretic force is responsible for the particle height bifurcation observed in some electrolytes. We demonstrate that at sufficiently low frequencies, particles suspended in electrolytes with large ionic mobility mismatches exhibit extreme levitation away from the electrode surface (up to 50 particle diameters). This levitation height scales approximately as the inverse square root of the frequency for both NaOH and KOH solutions. Moreover, larger particles levitate smaller distances, while the magnitude of the applied field has little effect above a threshold voltage. A force balance between the AREF-induced electrophoresis and gravity reveals saddle node bifurcations in the levitation height with respect to the frequency, voltage, and particle size, yielding stable fixed points above the electrode that accord with the experimental observations. These results point toward a low-energy, non-fouling method for concentrating colloids at specific locations far from the electrodes.

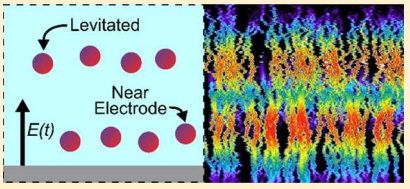

INTRODUCTION

The manipulation and control of colloidal systems using externally applied electric fields is a key component of numerous scientific applications, including the development of microfluidic devices and sensors,[1−4] photonic displays,[5] catalytic membranes,[6] high strength ceramics,[7,8] and techniques for wastewater separation.[9−11] In particular, the behavior of colloidal particles in close proximity to electrodes is of specific interest. Under applied ac fields, micron-scale particles suspended in electrolyte solutions near an electrode can exhibit planar aggregation[12−23] or separation[12,17,19−22] in the direction perpendicular to the applied field, as well as complex vertical motions parallel to the applied field.[24−26] Dutcher et al.[27] revealed that in NaCl, the vertical motion of these planar aggregates is dependent on the applied frequency of the system. At low frequencies, the average aggregate height above the electrode surface increases, resulting in changes in the aggregate morphology. Similarly, Saini et al.[23] observed changes in the aggregate height as a function of the electrolyte concentration and showed that the average aggregate height increases with decreasing concentration.

Recently, Woehl et al.[25] showed that in certain electrolytes (e.g., NaOH and HCl), particles can undergo a distinct height bifurcation into two stable average heights above the electrode. This behavior had not been observed with particles suspended in NaCl or KCl solutions. Specifically, upon application of the field, some of the particles moved closer to the electrode, while others moved upward to a new height, h (cf. Figure 1). They hypothesized that a radially inward electrohydrodynamic (EHD) flow generated on the electrode yields a vertical lift force that pushes particles away from the bottom[25,28] or top[28] of the electrode surface (depending on the electrode orientation),

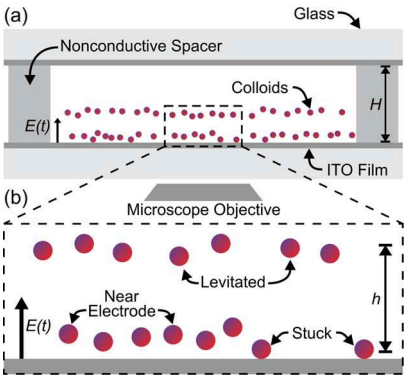

Figure 1. Experimental setup (a) cartoon of experimental setup showing particle height bifurcation after the application of an oscillatory electric field $E(t)$ (not to scale). (b) Magnification illustrates particles that are either levitated, near the electrode, or stuck (i.e., irreversibly adhered to the electrode). The average height (h) of the levitated particles varies with the applied frequency.

Received: January 31, 2019
Revised: April 29, 2019
Published: May 3, 2019

DOI: 10.1021/acs.langmuir.9b00313
Langmuir 2019, 35, 6971−6980

ultimately resulting in the pronounced height bifurcation. The balance between this EHD lift force and gravity resulted in the formation of a new "tertiary" energy minimum.

Subsequent work with a similar NaOH system revealed that at sufficiently low frequencies, particles can undergo height bifurcation while also simultaneously undergoing lateral aggregation near the electrode.[26] These results suggested that the key role of the surrounding electrolyte is to set the magnitude of the critical frequency (~25 Hz in 1 mM NaOH) at which particles transition between separating and aggregating behaviors. The existence of a critical aggregation frequency has since been corroborated by Ruud and Dutcher[28] who also showed that particles "levitated" away from the upper electrode as well to a stable height some distance beneath it. It should be noted that below the critical frequency, particles levitated out of the visible focal plane to extreme distances above the electrode.[26] These observations were later corroborated by Silvera Batista et al.[29] for surface modified particles in dc fields.

This extreme levitation is not readily explained by the height bifurcation mechanism originally proposed by Woehl et al.[25,28] Here, it was assumed that the EHD flow generates a vertical lift force on the particles causing them to levitate, and the magnitude of this predicted EHD flow was shown to decay as $\sim 1/h^3$. Thus, the vertical driving force for the height bifurcation would be negligible at such large reported distances (>10 particle diameters above the electrode[26,29]), suggesting that the EHD fluid flow is not the sole explanation for the particle height bifurcation.

Notably, previous efforts for interpreting the particle/electrolyte behavior used linearized forms of the standard electrokinetic model[30,31] to describe the electric field experienced by the particles. With the limit of small oscillatory potentials, the standard model predicts a sinusoidal electric field with a time-average of zero within the solution, that is, no net steady field component. Numerical computations of the fully non-linear electrokinetic model for electrolytes with equal ionic mobilities, however, show that the electric field takes on a much more complex shape (i.e., non-sinusoidal) at sufficiently high potentials.[32−34] Recent work by Hashemi Amrei et al.[35] expanded on these non-linear analyses to account for the effect of non-equal ionic mobilities. They demonstrated that a mismatch in the ionic mobilities leads to an uneven oscillation of ions, yielding a previously unanticipated steady component to the electric field. This steady, long-range "asymmetric rectified electric field" (AREF)[35] can, in turn, induce a constant electrophoretic force acting on a colloidal particle. Hashemi Amrei et al. provided a limited set of experimental measurements of the particle height bifurcation, demonstrating that for at least one particle type and electrolyte type, the experimental observations were qualitatively consistent with a model predicated on a balance between an AREF-induced electrophoretic force and gravity.

The main goal of this article is to provide a more detailed experimental and theoretical analysis of the particle height bifurcation behavior. Specifically, we report even more extreme particle levitation (up to 50 particle diameters) under low frequency oscillatory fields for several different particle sizes, frequencies, voltages, and electrolyte types. We develop a detailed model for the particle behavior in terms of an AREF-induced electrophoretic force balanced with the gravitational force on a particle, yielding a complex set of saddle-node bifurcations with stable and unstable fixed points for the particle height above the electrode. We used a confocal microscopy approach to test the model predictions, and we find that the experimental results accord with the theoretically predicted trends for frequency, particle size, and voltage. The findings presented here point toward a low-energy, non-fouling method for concentrating colloids at specific locations far from the electrodes.

THEORETICAL MODELING

Overview of the AREF. Full details of the AREF derivation are available from Hashemi Amrei et al.;[35] here, we provide a brief overview. The key and, perhaps, counterintuitive idea is that application of a perfectly sinusoidal potential to parallel electrodes yields an electric field with a steady component, as long as the electrolyte ions present have unequal mobilities. As discussed by Hashemi Amrei and colleagues, this steady field can be rationalized in terms of a simple two-ion model.[35] Here, two isolated oppositely charged ions oscillate in response to a sinusoidal field where ions with a larger radius have a larger drag coefficient and thereby, a slower ionic mobility. The mobility mismatch is defined as $\delta = a_+/a_-$ in terms of the ionic radii (a_i), or equivalently in terms of the Stokes−Einstein diffusion coefficients as $\delta = D_-/D_+$. The time-averaged perturbation of the electric field, $\langle \epsilon_z \rangle$, can then be solved by balancing the drag force with the electrostatic driving force and taking a Taylor series expansion of Coulomb's law[35] at distances far away from the oscillating dipoles. Qualitatively, when $\delta \neq 1$, the faster moving ion exhibits a higher amplitude than the slower ion, causing the center of charge in the system to oscillate. This asymmetric charge oscillation leads to a nonzero steady perturbation of the electric field $\langle \epsilon_z \rangle$ far from the charges, the magnitude of which scales as the square of the applied field strength, E_0^2 (cf. Figure 1, Hashemi Amrei et al.[35]).

Although this two-ion model captures why nonequal ionic mobilities can yield a steady field in response to an oscillating potential, the diffusive motion of the ions as well as ion−ion interactions must be accounted for to yield a realistic description of the electric field in an electrolyte solution. Accordingly, a full numerical solution of the standard electrokinetic model is required. The one-dimensional electric field for our electrolyte solution containing two ionic species, neglecting the presence of any colloidal particles, was calculated using the computational approach outlined by Hashemi Amrei et al.[35] Each ionic species (i) has a concentration n_i, radius a_i, and diffusivity defined as $D_i = k_B T/(6\pi\mu a_i)$, where k_B is the Boltzmann constant, T is temperature, and μ is the solution viscosity. The standard electrokinetic model couples Gauss's law

$$\varepsilon_\infty \varepsilon_0 \frac{\partial^2 \phi}{\partial z^2} = -\sum_{i=1}^{2} e q_i n_i \tag{1}$$

with the Nernst−Planck equation for each ionic species

$$\frac{\partial n_i}{\partial t} = D_i \frac{\partial^2 n_i}{\partial z^2} + e q_i \frac{D_i}{k_B T} \frac{\partial}{\partial z}\left(n_i \frac{\partial \phi}{\partial z} \right) \tag{2}$$

Here, ε_∞ and ε_0 are the solvent dielectric constant and vacuum permittivity, respectively, e is the elementary charge, and q_i is the charge number. The terms on the right side of eq 2 describe, respectively, the diffusive motion of the ions and the electromigration of the ions in response to the local electric field. Our system includes two parallel electrodes separated by a distance, H, subject to the following initial and boundary conditions

DOI: 10.1021/acs.langmuir.9b00313
Langmuir 2019, 35, 6971−6980

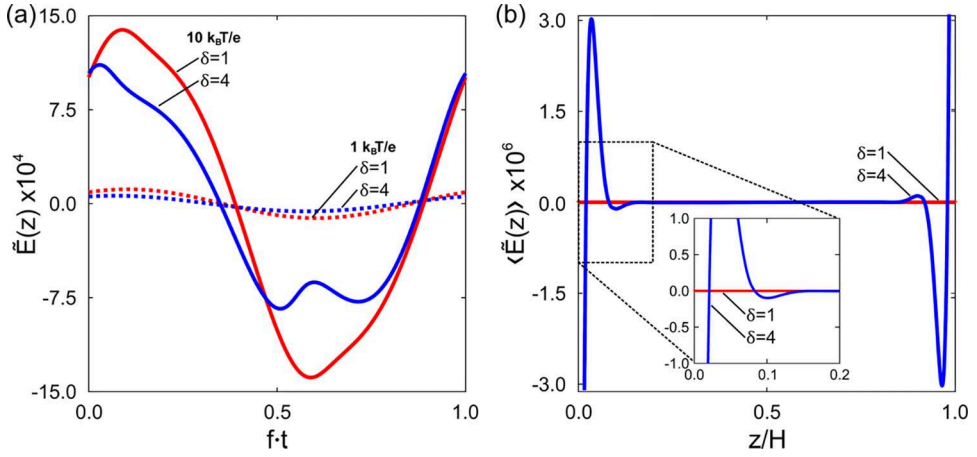

Figure 2. Calculated AREF. (a) Harmonic solutions for the normalized electric field vs time ($\tilde{E}(z) = E(z)e\kappa^{-1}/k_BT$) at $z = 1$ μm ($z/H = 0.02$). (b) Dimensionless time-averaged electric field, $\langle\tilde{E}(z)\rangle$, for different δ values. Parameters: $f = 500$ Hz, $\phi_o = 10\ k_BT/e$ (b), $H = 50$ μm, $\min(D_+,D_-) = 1 \times 10^{-9}$ m^2/s.

$$n_i(0, z) = n_i^{\infty} \tag{3a}$$

$$\phi(0, z) = 0 \tag{3b}$$

$$-D_i\left(\frac{\partial n_i}{\partial z} + \frac{eq_i n_i}{k_BT}\frac{\partial \phi}{\partial z}\right)_{z=0,H} = 0 \tag{3c}$$

$$\phi(t, 0) = \phi_0 \sin(\omega t), \qquad \phi(t, H) = 0 \tag{3d}$$

Initially, the system has an ion concentration equal to that of the bulk concentration, $n_i^{\infty} = n^{\infty}$ (eq 3a), with no applied potential (eq 3b). At each electrode, a no flux boundary condition is imposed such that no electrochemical reactions are present (eq 3c). Finally, at the lower electrode ($z = 0$), an oscillating potential is applied with a frequency and amplitude of $f = \omega/(2\pi)$ and ϕ_o, respectively, while the upper electrode remains grounded (eq 3d). We then solve the system of equations using finite difference and mesh refinement methods. No assumptions about the magnitude of the applied sinusoidal potential or about the mobilities of the ionic species were made.

Representative examples of the resulting normalized electric field ($\tilde{E}(z) = E(z)e\kappa^{-1}/k_BT$) are plotted versus time in Figure 2a for different values of δ and ϕ_o. At a low applied potential of 1 k_BT/e (dashed curves), $\tilde{E}(z)$ varies sinusoidally with time for both equal ($\delta = 1$) and unequal ($\delta = 4$) ionic mobilities. Similar to the previous non-linear analyses of the electrokinetic model,[32−34] as the applied potential is increased, the electric field acquires a more complex shape with several multi-modal peaks.[35] This behavior is exemplified using the solid curves in Figure 2a.

The corresponding time-averaged field, $\langle\tilde{E}(z)\rangle$, for $\phi_o = 10$ k_BT/e is plotted in Figure 2b as a function of the location between the electrodes (z). For equal ionic mobilities ($\delta = 1$), numerical integration yields a time-averaged field of zero everywhere within the solution. However, for a mismatch in the ionic mobilities ($\delta \neq 1$), the time-averaged field is non-zero which results in a steady AREF with complicated spatial dependence. Here, $\langle\tilde{E}(z)\rangle$ increases sharply from negative values near $z/H = 0$, passes through zero, reaches a maximum near $z/H = 0.04$, and then decreases and passes through zero a second time ($z/H = 0.08$) before leveling out above $z/H = 0.15$ (Figure 2b inset). At the opposite electrode, the negative mirror image of this behavior is observed. A key aspect of the steady AREF is that it persists over length scales well outside the Debye layer (located at $z/H < 0.0002$ and $z/H < 0.9998$ in Figure 2b for a Debye length of $\kappa^{-1} = 10$ nm). The characteristic length scale of the AREF outside the Debye layer is consistent with the scaling analysis of eq 2, where the characteristic time is chosen as the inverse frequency, yielding

$$L \propto \sqrt{D/\omega} \tag{4}$$

This characteristic distance over which the AREF peaks outside the Debye layer follows an inverse square root frequency dependence. Qualitatively speaking, as the applied frequency is decreased, the AREF moves further from the electrode surface. At higher frequencies, this characteristic length scale decreases, and the AREF oscillates spatially between positive and negative values more rapidly (i.e., there are more zeros of the electric field vs position).[35]

Force Balance on a Particle. Having established the existence of a long range electric field with a steady component but complicated spatial dependence, we now ask what the consequences will be for an individual colloid placed in that field. The strength of the EHD pseudo-potential derived by Woehl et al.,[25] as well as particle−electrode interactions (i.e., double layer repulsion and van der Waals attraction), are dependent on several individual system parameters including electrolyte type, ionic strength, particle size, zeta potential, applied voltage, and frequency. For previous experiments with 2 μm diameter particles in 1 mM NaOH under a 4 V_{pp}, 100 Hz electric field, the particle interaction potentials are all predicted to be less than 1 k_BT (the thermal energy) above more than 5 μm off the electrode surface.[25] However, particles were experimentally observed to move to heights upward of 8 μm where the EHD pseudo-potential is shown to be negligible.[25] Given this observation, we assume that particles are levitated sufficiently far from the electrode surface where the particle−electrode interactions can be neglected, and restrict our attention to an isolated colloid far from the electrode.

Experimentally, the particles are observed to move to a new height within a few seconds after application of the oscillatory potential, and these levitated particles remain at that height indefinitely while the field is applied. We ignore the initial brief transient behavior to focus on the force balance when the particles are stationary. Thus, the net time-averaged force on a particle is simply the balance between the AREF-induced

DOI: 10.1021/acs.langmuir.9b00313
Langmuir 2019, 35, 6971−6980

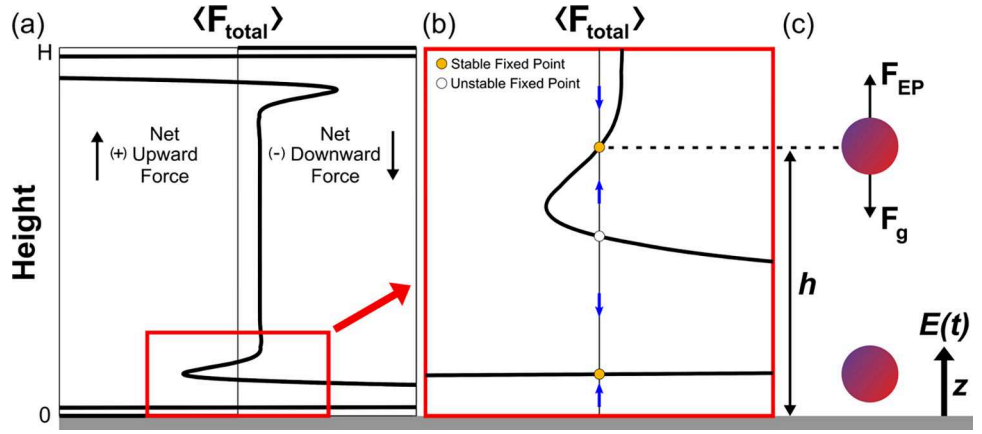

Figure 3. Total force diagram. (a) Cartoon schematic of the total force distribution resulting from a balance between the AREF-induced electrophoretic force and gravity. For negatively charged particles, a net upward force is felt when $\langle F_{total}\rangle > 0$. (b) Expanded view of the total force distribution showing multiple fixed points ($\langle F_{total}\rangle = 0$) at different heights above electrode. For visual understanding, the force diagrams in (a,b) are oriented vertically. (c) Particle height bifurcation to the predicted stable fixed point locations where the AREF-induced electrophoretic and gravitational forces balance.

electrophoretic driving force (F_{EP}, cf. refs 36 and 37) and the gravitational force (F_g) acting on the particle

$$\langle F_{tot}\rangle = F_{EP} + F_g = 6\pi a\varepsilon_\infty\varepsilon_0\zeta_P\langle E(z)\rangle - \frac{4}{3}\pi a^3\Delta\rho g \tag{5}$$

Here ζ_P is the zeta potential of the particle, $2a = d$ is the particle diameter, $\Delta\rho$ is the density difference between the particle and the fluid, and g is the acceleration due to gravity. We note that for our model system we assume a sufficiently thin electric double layer such that $\kappa a \gg 1$, so that F_{EP} in eq 5 is valid.[36,37] Figure 3a shows a representative example of the vertical force distribution predicted from eq 5. Steep changes in the predicted force, as well as multiple sign changes, are observed near both electrode surfaces. Specifically, the force at the bottom electrode changes the sign near the characteristic distance of $z \propto \sqrt{D/\omega}$. The long flat region throughout the middle of the cell, where the AREF is relatively weak, is mainly a result of the location-invariant gravitational force on the particle.

Our experimental work is focused on negatively charged particles; so we consider a negatively charged colloidal particle suspended between the electrodes at some vertical height, z. When $\langle F_{tot}\rangle > 0$ or $\langle F_{tot}\rangle < 0$, the particle experiences a net upward or downward force, respectively. Therefore, intersections with the equilibrium line ($\langle F_{tot}\rangle = 0$) provide the positions or fixed point locations, where the particle experiences zero net force. Three such fixed points are observed near the bottom electrode (magnification in Figure 3b). Importantly, the stability of these points alternates between stable and unstable. If the particles are initially positioned near an unstable fixed point when the field is applied, Brownian motion and the force distribution will cause them to move toward one of the neighboring stable fixed points, thereby inducing a height bifurcation (Figure 3c). The formation of multiple stable points above the electrode surface is qualitatively consistent with the existence of the apparent tertiary energy minimum that has been experimentally observed in the particle height bifurcation studies.[25,26]

To calculate the fixed point locations, we set $\langle F_{tot}\rangle$ in eq 5 equal to zero and solve for the time-averaged AREF. The resulting expression is given as

$$\langle E(z)\rangle = \frac{2\Delta\rho g a^2}{9\varepsilon_\infty\varepsilon_0\zeta_P} \tag{6}$$

where $\langle E(z)\rangle$ is a numerical expression with complicated spatial dependence (cf. Figure 2b). Equation 6 shows that at the fixed points, the magnitude of the AREF is proportional to the square of the particle size and inversely proportional to the zeta potential. Thus, an increase in a or a decrease in ζ_P will require a corresponding increase in the magnitude of $\langle E(z)\rangle$ in order for the particle to maintain its given stable position.

For the limiting case where the particles are density matched with the solvent (i.e. $\Delta\rho = 0$), the gravitational force disappears and eq 6 simplifies to

$$\langle E(z)\rangle = 0 \tag{7}$$

Therefore, for a density matched system, the positions of the stable points depend solely on the characteristics of $\langle E(z)\rangle$ and are independent of the particle size and zeta potential.

Because the electric field is complicated spatially and only calculable with numerical computations, it is not straightforward to solve eq 6 in a closed form. As a first order approximation for the complicated time-averaged AREF, we can take a Taylor series expansion of $\langle E(z)\rangle$ about a point z_f

$$\langle E(z)\rangle \approx \langle E(z_f)\rangle + \left.\frac{d\langle E\rangle}{dz}\right|_{z=z_f}(h - z_f) \tag{8}$$

where z_f is a zero of the electric field (i.e. $\langle E(z_f)\rangle = 0$). For example, in Figure 2b, the electric field approaches a zero value near $z_f = 0.15$. Substituting eq 8 in eq 6 and solving for the upper stable fixed point location, h, gives the resulting approximation

$$h \approx \frac{2\Delta\rho g a^2}{9\varepsilon_\infty\varepsilon_0\zeta_P\left.\frac{d\langle E\rangle}{dz}\right|_{z=z_f}} + z_f \tag{9}$$

In Figure 2b, as the approximated line approaches the point z_f, the slope $\left(\left.\frac{d\langle E\rangle}{dz}\right|_{z=z_f}\right)$ is observed to be positive while ζ_P is negative for the negatively charged particles in our system. As a result, the first term on the right hand side of eq 9 will be negative overall. Therefore, if the charge density remains constant, and as

DOI: 10.1021/acs.langmuir.9b00313
Langmuir 2019, 35, 6971−6980

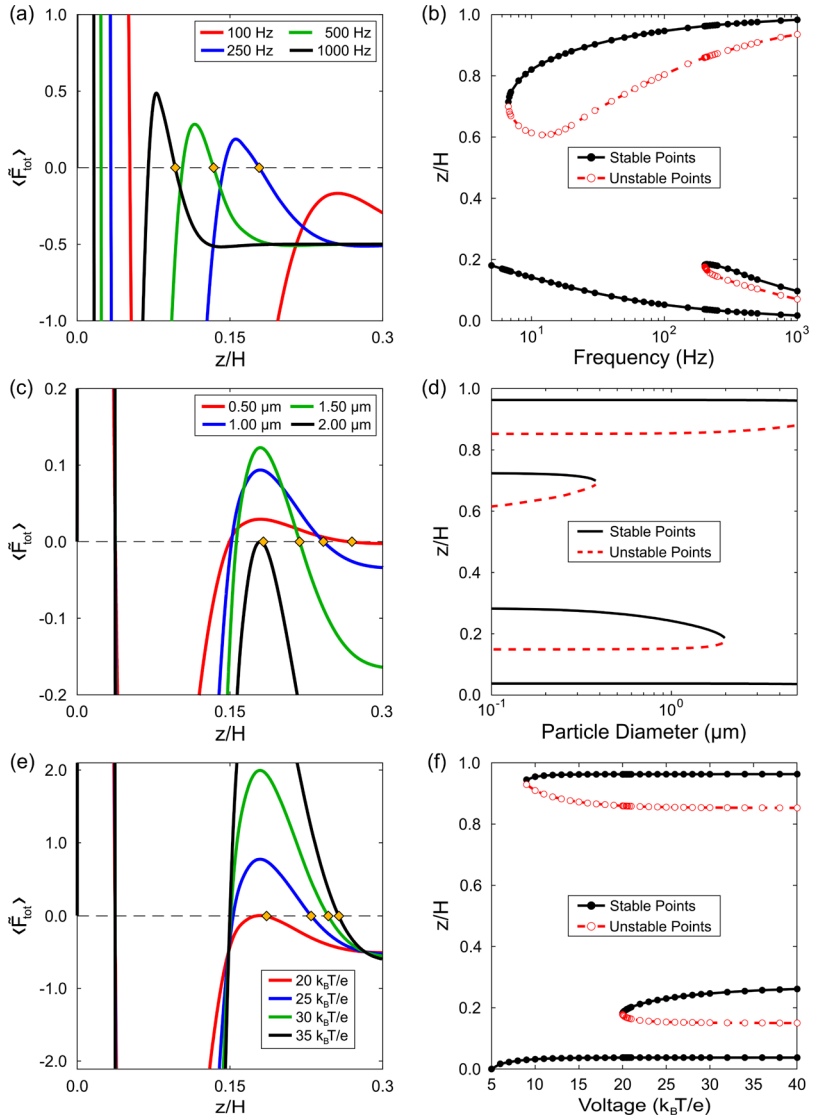

Figure 4. Theoretical particle height dependencies. Predicted AREF-induced force distributions ($\langle \tilde{F}_{tot} \rangle = \langle F_{tot} \rangle a/k_BT$) and the corresponding fixed point stability diagrams plotted as a function of frequency (f) (a,b), particle diameter (d) (c,d), and applied voltage (ϕ_o) (e,f). Yellow diamond markers (a,c,e) show the location of the upper stable fixed points and their dependence on each given variable. Parameters: $f = 200$ Hz (c–f), $\phi_o = 20\ k_BT/e$ (a–d), $H = 50\ \mu$m, $d = 2\ \mu$m (a,b,e,f), $\zeta_P = -110$ mV, $\delta = 3.97$.

the particle size is increased, the observed stable particle location will decrease—i.e. a heavier particle will sink down further than a lighter particle.

Predicted Levitation Height Dependencies. Based on the force balance mechanism described above, we can predict the effects of various system parameters on the particle height bifurcation/levitation behavior. The applied frequency and voltage are varied and the resulting time-averaged AREF is calculated using eqs 1 and 2. This corresponding $\langle E(z) \rangle$ is then substituted in eq 5 to solve the total force distribution on a negatively charged particle with a varying size, and the theoretical results for the predicted AREF-induced force distributions are plotted in Figure 4. It should be noted that computational limitations required the modeled system to be scaled down from the experimental setup and prevented direct 1:1 comparisons; qualitative comparisons, however, provide useful insights into the particle height dependence as a function of the varying system parameters. (More details on these limitations are discussed below). Similar to Figure 3b, we see that the total force for each varying parameter (Figure 4a,c,e) increases and decreases sharply from $z/H = 0$ with a large maximum near the electrode surface followed by a deep minimum after passing through zero. Following this minimum, the force passes through zero a second time and reaches a local positive maximum before decreasing and finally becoming negative. The yellow diamond markers in Figure 4a,c,e denote the location of the upper fixed point near the bottom electrode where the force passes through zero for the third time. A similar trend is observed near the top electrode (not pictured in Figure 4).

From Figure 4a, it can be predicted that as the frequency is decreased, the height of the stable point increases and particles are expected to levitate farther from the electrode surface. At 100 Hz, the predicted force distribution shows only one stable point near the bottom electrode at $z/H = 0.05$. A further fixed point analysis shows the behavior of the stable and unstable points over an expanded range of frequencies. Open red markers and closed black markers in Figure 4b denote unstable and stable

DOI: 10.1021/acs.langmuir.9b00313
Langmuir 2019, 35, 6971−6980

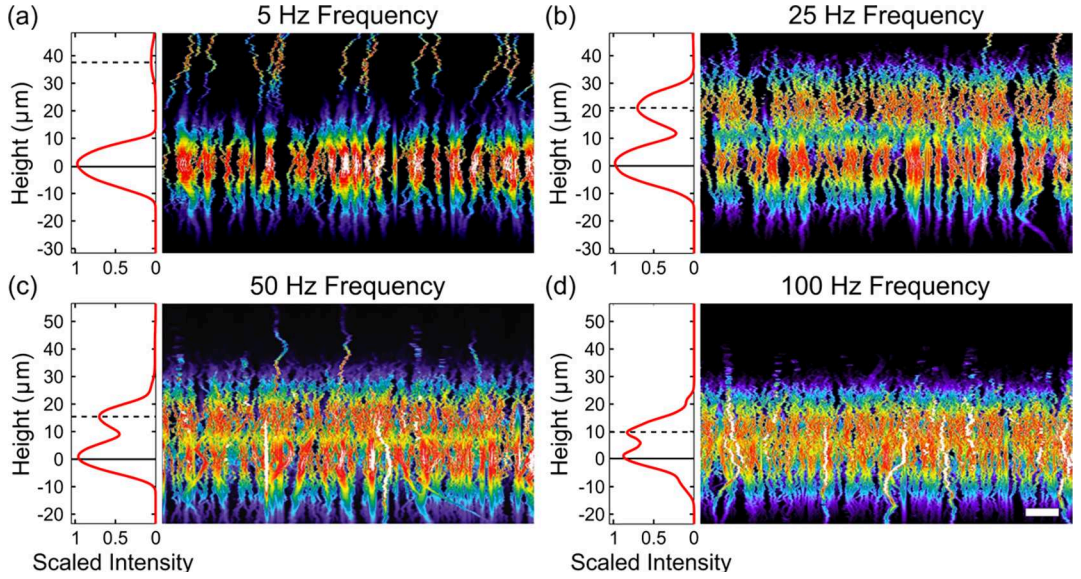

Figure 5. Representative confocal cross-sections. False-colored confocal z-stacks of PS particles suspended in 1 mM NaOH. The color intensity corresponds to the fluorescent intensity of the individual colloids which follows a Lorentzian distribution. This results in the vertical elongation of the particles. (a) At 5 Hz, two distinct planes of particles are observed with the upper plane of particles levitating nearly 40 μm. As the frequency is increased to (b) 25, (c) 50, and (d) 100 Hz the levitation height decreases to ~8 μm above the electrode surface. Scale bar is 10 μm. Parameters: $\phi_{pp} = 4$ V_{pp}, $H = 1000$ μm, $d = 2$ μm.

fixed points, respectively. Here, the frequency is varied from 5−1000 Hz, revealing three interesting regimes. First, at frequencies below 6 Hz, only one stable fixed point exists near the bottom electrode. As the frequency is increased above 6 Hz, a saddle node bifurcation occurs, with a second stable fixed point along with one unstable fixed point appearing near the top electrode. Increasing the frequency further to ~200 Hz results in an additional saddle node point near the bottom electrode. Analogous to Figure 3, one unstable and two stable fixed points now exist near the bottom electrode. For example, at 500 Hz, a particle initially located at $z/H < 0.10$ or $z/H > 0.10$ will either move downward toward the stable fixed point near the electrode or levitate upward toward the stable point near $z/H = 0.15$, respectively. This type of bifurcation in the particle height is seen qualitatively in experiments.[25,26] A power law fit of the upper stable fixed points yields a frequency dependence of $\omega^{-0.5}$ over the range of 300−1000 Hz—the same as the predicted AREF length scale of $\omega^{-1/2}$ (cf. eq 4).

The predicted upper bifurcation height is also observed to be negatively correlated with changes in the particle size (Figure 4c). Because F_g has a cubic dependence on the particle diameter compared to a linear dependence on the electrophoretic force F_{EP}, the effects of gravity are more pronounced for larger particles. Therefore, as the diameter increases, particles feel a stronger downward gravitational force, and the stable point moves closer to the electrode surface (cf. eqs 6 and 8). Contrarily, for the same frequency and voltage, smaller particles are expected to levitate to larger distances above the electrode surface. Figure 4d shows the effect of the varying particle size from diameters of 0.1−5 μm (open and closed markers are not shown for clarity where the particle diameter is varied analytically via eq 6). Similar to the frequency trend above, for sufficiently small diameters (<2 μm), multiple stable fixed points form near the bottom electrode. Continuing to decrease the diameter down to ~0.4 μm results in the formation of a saddle node and two additional fixed points above $z/H = 0.6$. In this state, particles could theoretically show a similar height bifurcation behavior near the top electrode. Above 2 μm, a saddle node appears and the system loses one stable and one unstable fixed point near the bottom electrode. Here, the effect of gravity on larger particles is strong enough to overcome the long-range AREF-induced force, and no height bifurcation is expected.

Finally, Figure 4e,f show the effect of varying the applied potential. As the strength of the applied potential is increased, the location of the stable fixed point moves farther from the electrode surface. Only slight changes in this stable point location are predicted for further voltage increases. Like the aforementioned trends, the fixed point diagram in Figure 4f shows that a particle height bifurcation state occurs given sufficiently large potentials (>20 k_BT/e). Below 20 k_BT/e, there is only one stable fixed point near the bottom electrode. Similar to larger particles, the AREF-induced force is not strong enough to induce levitation if the applied voltage is too low, and height bifurcation will not be expected.

EXPERIMENTAL COMPARSIONS

Experimental Methods. To test the hypothesis that AREF-induced electrophoresis is responsible for the observed particle levitation, we performed a detailed series of height bifurcation experiments using confocal microscopy. Similar to previous work,[23,25,26,35] the present experimental devices were fabricated using two indium tin oxide electrodes (ITO, 5−15 Ω sheet resistance) separated using an $H = 1$ mm thick nonconductive polydimethylsiloxane spacer (Figure 1). Before device assembly, the electrodes were washed and ultrasonicated for 10 min each in RBS 35 detergent, acetone, and deionized (DI) water, respectively.

Suspensions of fluorescent sulfonated polystyrene (PS) particles (diameter, $d = 1$, 2, or 4 μm) were prepared in 1 mM NaOH and KOH (conductivity, $\sigma_{NaOH} \cong 245$ μS/cm and $\sigma_{KOH} \cong 250$ μS/cm) using DI water (18.2 MΩ·cm). First, the particles were washed via centrifugation and resuspension, and then diluted to a volume fraction of 3×10^{-4}. Next, the electrophoretic mobility (u_e) of these particles was measured using dynamic light scattering (Malvern Zetasizer), and the zeta potential for both NaOH and KOH was approximated using the Helmholtz−Smoluchowski relation for small mobilities as −110 and

DOI: 10.1021/acs.langmuir.9b00313
Langmuir 2019, 35, 6971−6980

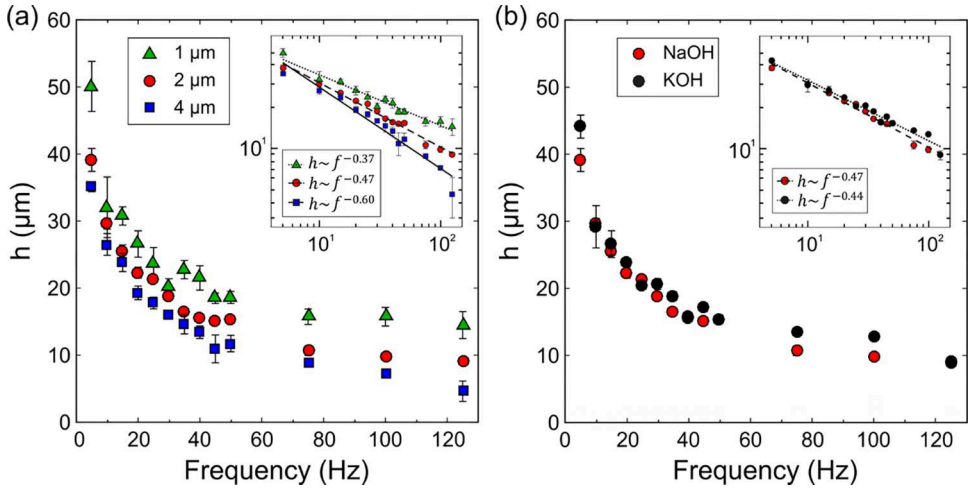

Figure 6. Applied frequency dependence. (a) Levitated particle height vs applied frequency for 1, 2, and 4 μm diameter colloidal particles. (Inset) log−log plot showing the particle height dependence on the applied frequency for each particle size. (b) Comparison between NaOH and KOH electrolytes. (Inset) log−log plot of height vs frequency for each electrolyte. 2 μm diameter NaOH data [red circles (a,b)] is reproduced from Hashemi Amrei et al.[35] Error bars for each data point are two standard deviations of the mean of at least three trial replicates. Parameters: ϕ_{pp} = 4 V_{pp}, H = 1000 μm, d = 2 μm (b), δ = 3.96 (NaOH) and 2.69 (KOH).

−114 mV, respectively. The corresponding δ-values calculated using the limiting conductance of each electrolyte ion were 3.96 for NaOH and 2.69 for KOH.[38]

To begin an experiment, 50 μL of a suspension was first placed on the bottom electrode and allowed to dry overnight, causing particles to irreversibly adhere to the electrode surface. These "stuck" particles were identified by their lack of Brownian motion (Figure 1b). A fresh particle suspension was then added to the fluid well and particles were allowed to settle by gravity for ∼2 h. After the smaller 1 and 2 μm particles settled near the bottom electrode, they continued to move laterally via Brownian motion indicating that they remained separated from the electrode surface by colloidal scale forces.

Once the particles were settled by gravity near the electrode surface, a function generator applied an oscillatory field with a specific voltage and frequency ranging from ϕ_{pp} = 1−4 V peak-to-peak (V_{pp}) and f = 5−125 Hz, respectively. The corresponding current magnitudes were similar to those reported previously.[26] The 1 and 2 μm particles were observed to move upward against gravity in response to the applied potential. For the larger 4 μm particles, though, the electric field was apparently not strong enough to overcome the gravitational force, and the electric field was applied prior to sedimentation; these particles sedimented under the influence of both gravity and the applied field.

A standard z-stack of images was collected using a laser scanning confocal microscope (Zeiss LSM 700) with a 0.2 μm step size (∼1 s/step) over an 80 μm tall region near the bottom electrode. Thus, each scan took ∼400 s to complete. Cross-sections of the compiled z-stack were then projected in the xz-plane in order to observe the fluorescence intensity as a function of height (Figure 5). Here, the color intensity corresponds to the fluorescence intensity of the individual colloids, each of which individually follows the Lorentzian distribution.[39] This distribution results in the apparent vertical elongation of the particles, while the Brownian motion of particles during scans causes the rippled (or "wiggly") appearance of each individual intensity profile. In other words, a single isolated particle appears as a vertical line. The full width half maximum of these individual Lorentzian profiles is controlled by the size of the confocal pinhole which was set to an optimum diameter of 1 Airy unit.[40] Additionally, small variations in the height of the particles in each vertical band will broaden the overall summed intensities (Figure 5). If all the particles remain at exactly the same vertical position, the peak will appear narrower than if the heights of the particles fluctuate near some average height. The stuck reference particles, however, exhibited no Brownian motion and could be easily identified to locate the electrode surface and establish a zero reference height (z = 0). Once the reference height was known, the z-stack was integrated along the x-direction to give the total fluorescence intensity as a function of height above the electrode. Thus, peaks in the maximum intensity corresponded to the average heights of each particle band—those near the electrode surface and those levitated to an extreme height, h (cf. Figure 1).

Effects of the Applied Field and Particle Size on Levitation. Figure 5 shows false-colored confocal z-stack cross-sections representative of height bifurcated particles in response to a 4 V_{pp} field. The fluorescence intensity profile of each plane of particles is shown as a function of the vertical z-position, and the corresponding integrated intensity distribution is plotted at the left. Peaks in the fluorescence intensity, therefore, correspond to the average center height of particles in that plane, with the magnitude of the peak proportional to the total number of particles that reside at that location. Upon application of a 5 Hz ac field (Figure 5a), the particles bifurcated into two distinct populations over approximately 10 s. Here, the levitation height (h) was nearly 40 μm off the electrode surface. The two populations of particles maintained stable heights and continued to exhibit Brownian motion until the applied electric field was removed. As the frequency was increased from 5 to 25, 50, and 100 Hz (Figure 5b−d), the corresponding levitation height decreased by a factor of four to approximately 10 μm, while the number of levitated particles noticeably increased. It should be noted, as reported by Bukosky and Ristenpart,[26] that particles in the lower plane readily formed large planar aggregates below the critical aggregation frequency. Above this critical frequency,[26] lateral separation occurs, and a larger fraction of particles are observed to levitate. We emphasize that after the initial height bifurcation, particles remained stable at their respective heights throughout the duration of the experiment, and no particles were observed to transition between the upper and lower heights.

To understand the effect of the electric field on the levitation height, confocal z-scans were recorded while systematically varying the frequency, particle diameter, and voltage. Figure 6a shows h as a function of frequency for 1, 2, and 4 μm sized PS particles (data for d = 2 μm is reproduced from Hashemi Amrei et al.[35]). As the frequency decreased from 125 to 5 Hz, the particle height increased significantly. For 2 μm particles, the corresponding maximum levitation height reached ∼20 particle diameters off the electrode surface (∼40 μm absolute height). The other particle sizes (d = 1 and 4 μm) qualitatively follow the same trends, with smaller particles systematically reaching larger levitation heights. In fact, at low frequencies the 1 μm diameter particles reached extreme heights of up to 50 particle diameters above the electrode. Separate power law fits of the height versus frequency data in Figure 6a indicate that h scaled as approximately $f^{-0.4}$–$f^{-0.6}$

DOI: 10.1021/acs.langmuir.9b00313
Langmuir 2019, 35, 6971−6980

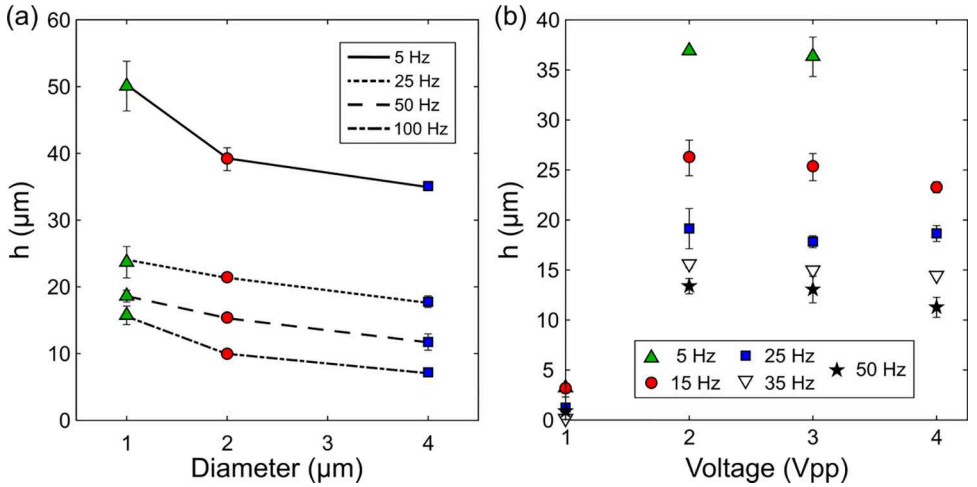

Figure 7. Size and voltage dependencies. (a) Levitated particle height vs particle diameter for 5, 25, 50, and 100 Hz applied frequencies. 2 μm diameter data (red circles) is reproduced from Hashemi Amrei et al.[35] (b) Particle height vs applied voltage for frequencies ranging from 5 to 50 Hz. At low frequencies and high voltages particles tended to adhere to the bottom electrode before height bifurcation could occur. Error bars for each data point are two standard deviations of the mean of at least three trial replicates. Parameters: $\phi_{pp} = 4\ V_{pp}$ (a), $H = 1000\ \mu$m (a) and 500 μm (b), $d = 2\ \mu$m (b), $\delta = 3.96$ (NaOH).

(Figure 6a inset), qualitatively consistent with the modeling results shown in Figure 4b where $h \approx \omega^{-0.5}$ as well as the AREF scaling where $z/H \propto \sqrt{2\pi D/(fH^2)}$; that is $z \propto f^{-1/2}$.

A similar frequency dependence was also observed for 2 μm diameter particles suspended in a KOH electrolyte solution (Figure 6b). Despite a difference in the δ-values for KOH and NaOH, the measured levitation heights as well as the inverse frequency trends showed good agreement with each other (Figure 6b inset). This experimentally observed behavior is consistent with the difference in the fixed point locations predicted for NaOH and KOH solutions. For example, under the same field conditions and electrode spacing, the upper stable fixed point is predicted to only differ by ~11%, where $z/H_{NaOH} = 0.25$ and $z/H_{KOH} = 0.28$ (see Supporting Information Figure S1). It should, however, be noted that because of computational limitations, the experimentally applied voltages for the data in Figure 6 were much higher than the simulated voltages in Figure 4.

Figure 7a shows the levitation height as a function of the particle diameter for various frequencies. Here, smaller particles are always observed to reach larger levitation heights across all frequencies (Figure 7a). For example, levitation heights are observed to decrease by ~20–30% when the particle diameter is doubled from 1 to 2 μm and from 2 to 4 μm. This experimental trend agrees with predictions based on eq 9 for the levitation height of a negatively charged particle in a $\phi_o = 20\ k_BT/e, f = 200$ Hz electric field. Here, doubling the particle diameter from 0.5 to 1 μm similarly predicts an ~10% decrease in the levitation height, but further increasing the particle size to 2 μm decreases the expected height by more than 35%. This large height decrease could be because of the difference between the small applied potentials used in the theoretical modeling compared to the significantly larger potentials used experimentally. For larger particles, the gravitational term in eq 5 will dominate if the magnitude of the AREF is small. However, if the applied potential is increased, the magnitude of the AREF-induced electrophoretic force would become comparable to the gravitational force and the corresponding levitation height would increase accordingly. Thus, the height prediction from eq 9 agrees with the experimental trends for sufficiently small particle diameters, but deviates for larger diameters.

Figure 7b shows the particle height as a function of voltage for various frequencies. Initially, particles remain close to the bottom electrode, but once the applied potential reaches some minimum threshold (between 1 and 2 V_{pp} for the given experimental conditions), height bifurcation occurs. Further increases in the voltage, however, had little effect on the maximum particle height. Recalling Figure 4e,f, a qualitatively similar plateau was theoretically shown above ~30 k_BT/e. Above this voltage, less than a 5% increase was predicted for the fixed point location. Because the experimentally applied voltages were significantly higher than the model predictions, but the same invariant behavior was observed, these experimental results corroborate the predicted voltage trend.

DISCUSSION AND CONCLUSIONS

In summary, we demonstrate that micrometer-scale particles suspended in electrolytes with a large ionic mobility mismatch will undergo extreme levitation in response to oscillatory electric fields. Direct height measurements using confocal microscopy show that at sufficiently low frequencies, particles can move upward to heights of more than 50 particle diameters away from the electrode surface. It is further demonstrated that such a particle behavior is consistent with a new mechanism based on AREFs. The resulting total force on a particle due to the balance of AREF-induced electrophoresis and gravity corroborates the existence of a tertiary energy minimum with multiple stable fixed points above the electrode, consistent with the experimentally observed height bifurcation and levitation.

Theoretical modeling and fixed point analyses were conducted by varying the applied frequency, voltage, and particle size. These theoretical results and predicted trends are qualitatively consistent with the experimental observations. For both NaOH and KOH electrolyte solutions, the levitation height was shown to scale approximately as the inverse square root of the frequency ($\sim f^{-1/2}$). This negative correlation between the particle size and the levitation height predicted by eq 9 was supported experimentally, where larger particles were systematically observed to levitate smaller distances. Finally, consistent with the predicted voltage dependency, the magnitude of the experimentally applied potential was observed to have a weak effect above a threshold voltage. The previously proposed EHD flow mechanism for particle height bifurcation[25,28] fails to capture these observed dependencies and is unable to account for the extreme levitation heights measured experimentally.

Several underlying assumptions of this newly proposed AREF model still remain unverified and require further consideration. Derivation of the AREF, for example, assumes that no chemical reactions occur near the electrode, a condition that is not

DOI: 10.1021/acs.langmuir.9b00313
Langmuir 2019, 35, 6971–6980

necessarily satisfied at low frequencies and high applied potentials. The presence of electrochemical reactions may induce other types of electrically generated fluid flows (such as induced charge electroosmosis[41−43] and faradaically coupled electroosmotic flow[43]). In principle, the presence of the AREF could also affect the local ion concentration and, thus, alter particle's Debye length and zeta potential. However, at the highest simulated potential ($40\ k_BT/e$), the local ion concentration is estimated to vary by less than 4% with changes in the Debye length of less than 2%. Thus, for the numerical results presented here, we neglected any impact on the change in salt concentration on the Debye layer. At higher applied voltages this change in concentration may be more significant. Moreover, the force balance presented in eq 5 is restricted to an isolated particle far from the electrode surface. Future numerical calculations should account for both particle−particle and particle−electrode interactions, as well as changes in the local ion concentration.

Finally, with the current numerical algorithm and available computational power, obtaining harmonic solutions at an applied potential of $V = 0.25\ V_{pp}$ over an electrode spacing of $H = 50\ \mu m$ required approximately 7 days of CPU time. Because the computational time scales roughly as $(\kappa H)^2$, we estimate that obtaining a convergent harmonic solution for the experimental parameters at $V = 4\ V_{pp}$ and $H = 1$ mm would require more than 7 years using our current computational capabilities. Given this estimate, 1:1 experimental comparisons are not feasible with the current numerical capabilities. Even though the proposed mechanism agrees qualitatively well with experimentally observed particles in ac fields, more robust and detailed computations are needed for direct numerical comparisons.

The theoretical modeling also predicted multiple fixed points located near the top electrode surface; however, our results presented here only focus on the particle behavior at the lower electrode. Recent experiments by Ruud and Dutcher[28] showed evidence to corroborate these predictions, but further experimentation is necessary in order to fully characterize the behavior of particles near the top electrode surface. Likewise, the role that individual ions have in the behavior of the particles remains obscure. To our knowledge, the particle height bifurcation phenomenon has only been observed in electrolytes containing H^+ or OH^-. It is well known that these ions have large mobilities because of their ability to transport quickly through networks of hydrogen bonds via the Grotthuss mechanism.[44] It is unclear whether the height bifurcation is a result of the Grotthuss mechanism of H^+/OH^- transport, or the magnitude of the δ-mismatch regardless of the identity of the ion. Therefore, additional experimental studies should be performed to systematically test a broad selection of electrolytes with varying mobility mismatches in order to better understand the impact of the individual ions.

Future work should also involve expanding the total force balance in eq 5 to include additional contributions for the effects of varying particle shapes and surface asymmetries such as patchy colloids,[45−47] Janus particles,[29,48] colloidal dimers,[49,50] and so forth. Asymmetries in the orientation of the electrodes themselves have also been shown to play a key role in the particle separation behavior.[12] Likewise, the effects of varying electrode geometries on the resulting AREF should be further explored. A key practical implication of our results is that under appropriate conditions, particles levitate to extreme heights above the electrode surface. This phenomenon could be particularly useful as a way to manipulate particles in lab-on-chip applications. For example, it is expected that particles with differing size, shape, and/or surface charge will levitate to varying equilibrium heights for the same applied field. Thus, one could imagine using an ac field to rapidly separate mixtures of particles into different streams or channels. Likewise, if the electric field is applied to a dispersed suspension of particles, one could drive sedimentation to a specific location. Unlike traditional electrophoretic deposition techniques using dc fields, this ac field approach points toward a low-energy, non-fouling method for concentrating and "trapping" colloids far from the electrodes. This technique may potentially be of interest for applications involving deposition at a liquid−liquid interface, or even as a method for concentrating functionalized particles for targeted delivery.

■ ASSOCIATED CONTENT

Supporting Information

The Supporting Information is available free of charge on the ACS Publications website at DOI: 10.1021/acs.langmuir.9b00313.

Predicted AREF-induced force distributions comparing NaOH and KOH electrolyte solutions (PDF)

■ AUTHOR INFORMATION

Corresponding Authors

*E-mail: grgmiller@ucdavis.edu (G.H.M.).
*E-mail: wdristenpart@ucdavis.edu (W.D.R.).

ORCID

Scott C. Bukosky: 0000-0001-7075-3276
William D. Ristenpart: 0000-0002-4935-6310

Author Contributions

§S.C.B. and S.M.H.H.A. contributed equally to this work.

Notes

The authors declare no competing financial interest.

■ ACKNOWLEDGMENTS

Work by S.C.B. was performed under the auspices of the U.S. Department of Energy by Lawrence Livermore National Laboratory under contract DE-AC52-07NA27344. LLNL-JRNL-758401. S.M.H.H.A. was partially supported by the National Science Foundation under grant no. DMS-1664679.

■ REFERENCES

(1) Gupta, S.; Alargova, R. G.; Kilpatrick, P. K.; Velev, O. D. On-Chip Electric Field Driven Assembly of Biocomposites from Live Cells and Functionalized Particles. *Soft Matter* **2008**, *4*, 726−730.

(2) Marín-Suárez, M.; Medina-Rodríguez, S.; Ergeneman, O.; Pané, S.; Fernández-Sánchez, J. F.; Nelson, B. J.; Fernández-Gutiérrez, A. Electrophoretic Deposition as a New Approach to Produce Optical Sensing Films Adaptable to Microdevices. *Nanoscale* **2013**, *6*, 263−271.

(3) Gabardo, C. M.; Soleymani, L. Deposition, Patterning, and Utility of Conductive Materials for the Rapid Prototyping of Chemical and Bioanalytical Devices. *Analyst* **2016**, *141*, 3511−3525.

(4) Salafi, T.; Zeming, K. K.; Zhang, Y. Advancements in microfluidics for nanoparticle separation. *Lab Chip* **2016**, *17*, 11−33.

(5) Nucara, L.; Greco, F.; Mattoli, V. Electrically Responsive Photonic Crystals: A Review. *J. Mater. Chem. C* **2015**, *3*, 8449−8467.

(6) Shan, W.; Zhang, Y.; Yang, W.; Ke, C.; Gao, Z.; Ye, Y.; Tang, Y. Electrophoretic Deposition of Nanosized Zeolites in Non-Aqueous Medium and Its Application in Fabricating Thin Zeolite Membranes. *Microporous Mesoporous Mater.* **2004**, *69*, 35−42.

DOI: 10.1021/acs.langmuir.9b00313
Langmuir 2019, 35, 6971−6980

(7) Sarkar, P.; De, D.; Rho, H. Synthesis and Microstructural Manipulation of Ceramics by Electrophoretic Deposition. *J. Mater. Sci.* **2004**, *39*, 819−823.
(8) Novak, S.; Iveković, A. Fabrication of SiCf/SiC Composites by SITE-P Process. *J. Nucl. Mater.* **2012**, *427*, 110−115.
(9) Ichikawa, T.; Itoh, K.; Yamamoto, S.; Sumita, M. Rapid Demulsification of Dense Oil-in-Water Emulsion by Low External Electric Field. *Colloids Surf., A* **2004**, *242*, 21−26.
(10) Vigo, C. R.; Ristenpart, W. D. Aggregation and Coalescence of Oil Droplets in Water via Electrohydrodynamic Flows. *Langmuir* **2010**, *26*, 10703−10707.
(11) Zhang, H.; Bukosky, S. C.; Ristenpart, W. D. Low-Voltage Electrical Demulsification of Oily Wastewater. *Ind. Eng. Chem. Res.* **2018**, *57*, 8341−8347.
(12) Gong, T.; Wu, D. T.; Marr, D. W. M. Two-Dimensional Electrohydrodynamically Induced Colloidal Phases. *Langmuir* **2002**, *18*, 10064−10067.
(13) Ristenpart, W. D.; Aksay, I. A.; Saville, D. A. Electrically Guided Assembly of Planar Superlattices in Binary Colloidal Suspensions. *Phys. Rev. Lett.* **2003**, *90*, 128303.
(14) Trau, M.; Saville, D. A.; Aksay, I. A. Field-Induced Layering of Colloidal Crystals. *Science* **1996**, *272*, 706−709.
(15) Trau, M.; Saville, D. A.; Aksay, I. A. Assembly of Colloidal Crystals at Electrode Interfaces. *Langmuir* **1997**, *13*, 6375−6381.
(16) Gong, T.; Marr, D. W. M. Electrically Switchable Colloidal Ordering in Confined Geometries. *Langmuir* **2001**, *17*, 2301−2304.
(17) Kim, J.; Anderson, J. L.; Garoff, S.; Sides, P. J. Effects of Zeta Potential and Electrolyte on Particle Interactions on an Electrode under Ac Polarization. *Langmuir* **2002**, *18*, 5387−5391.
(18) Kim, J.; Guelcher, S. A.; Garoff, S.; Anderson, J. L. Two-Particle Dynamics on an Electrode in Ac Electric Fields. *Adv. Colloid Interface Sci.* **2002**, *96*, 131−142.
(19) Ristenpart, W. D.; Aksay, I. A.; Saville, D. A. Assembly of Colloidal Aggregates by Electrohydrodynamic Flow: Kinetic Experiments and Scaling Analysis. *Phys. Rev. E: Stat., Nonlinear, Soft Matter Phys.* **2004**, *69*, 021405.
(20) Hoggard, J. D.; Sides, P. J.; Prieve, D. C. Electrolyte-Dependent Pairwise Particle Motion near Electrodes at Frequencies below 1 KHz. *Langmuir* **2007**, *23*, 6983−6990.
(21) Hoggard, J. D.; Sides, P. J.; Prieve, D. C. Electrolyte-Dependent Multiparticle Motion near Electrodes in Oscillating Electric Fields. *Langmuir* **2008**, *24*, 2977−2982.
(22) Wirth, C. L.; Rock, R. M.; Sides, P. J.; Prieve, D. C. Single and Pairwise Motion of Particles near an Ideally Polarizable Electrode. *Langmuir* **2011**, *27*, 9781−9791.
(23) Saini, S.; Bukosky, S. C.; Ristenpart, W. D. Influence of Electrolyte Concentration on the Aggregation of Colloidal Particles near Electrodes in Oscillatory Fields. *Langmuir* **2016**, *32*, 4210−4216.
(24) Fagan, J. A.; Sides, P. J.; Prieve, D. C. Vertical Oscillatory Motion of a Single Colloidal Particle Adjacent to an Electrode in an Ac Electric Field. *Langmuir* **2002**, *18*, 7810−7820.
(25) Woehl, T. J.; Chen, B. J.; Heatley, K. L.; Talken, N. H.; Bukosky, S. C.; Dutcher, C. S.; Ristenpart, W. D. Bifurcation in the Steady-State Height of Colloidal Particles near an Electrode in Oscillatory Electric Fields: Evidence for a Tertiary Potential Minimum. *Phys. Rev. X* **2015**, *5*, 011023.
(26) Bukosky, S. C.; Ristenpart, W. D. Simultaneous Aggregation and Height Bifurcation of Colloidal Particles near Electrodes in Oscillatory Electric Fields. *Langmuir* **2015**, *31*, 9742−9747.
(27) Dutcher, C. S.; Woehl, T. J.; Talken, N. H.; Ristenpart, W. D. Hexatic-to-Disorder Transition in Colloidal Crystals Near Electrodes: Rapid Annealing of Polycrystalline Domains. *Phys. Rev. Lett.* **2013**, *111*, 128302.
(28) Ruud, E. D.; Dutcher, C. S. Electrohydrodynamic Aggregation with Vertically Inverted Systems. *Phys. Rev. E* **2018**, *97*, 022614.
(29) Silvera Batista, C. A.; Rezvantalab, H.; Larson, R. G.; Solomon, M. J. Controlled Levitation of Colloids through Direct Current Electric Fields. *Langmuir* **2017**, *33*, 10861−10867.
(30) O'Brien, R. W.; White, L. R. Electrophoretic Mobility of a Spherical Colloidal Particle. *J. Chem. Soc., Faraday Trans. 2* **1978**, *74*, 1607−1626.
(31) DeLacey, E. H. B.; White, L. R. Dielectric Response and Conductivity of Dilute Suspensions of Colloidal Particles. *J. Chem. Soc., Faraday Trans. 2* **1981**, *77*, 2007−2039.
(32) Højgaard Olesen, L.; Bazant, M. Z.; Bruus, H. Strongly Nonlinear Dynamics of Electrolytes in Large Ac Voltages. *Phys. Rev. E: Stat., Nonlinear, Soft Matter Phys.* **2010**, *82*, 011501.
(33) Schnitzer, O.; Yariv, E. Nonlinear Oscillations in an Electrolyte Solution under Ac Voltage. *Phys. Rev. E: Stat., Nonlinear, Soft Matter Phys.* **2014**, *89*, 032302.
(34) Stout, R. F.; Khair, A. S. Moderately Nonlinear Diffuse-Charge Dynamics under an Ac Voltage. *Phys. Rev. E: Stat., Nonlinear, Soft Matter Phys.* **2015**, *92*, 032305.
(35) Hashemi Amrei, S. M. H.; Bukosky, S. C.; Rader, S. P.; Ristenpart, W. D.; Miller, G. H. Oscillating Electric Fields in Liquids Create a Long-Range Steady Field. *Phys. Rev. Lett.* **2018**, *121*, 185504.
(36) Russel, W. B.; Saville, D. A.; Schowalter, W. R. *Colloidal Dispersions; Cambridge Monographs on Mechanics*; Cambridge University Press, 1989.
(37) Masliyah, J. H.; Bhattacharjee, S. *Electrokinetic and Colloid Transport Phenomena*; John Wiley & Sons, Inc.: Hoboken, NJ, 2006.
(38) Hollingsworth, A. D.; Saville, D. A. A Broad Frequency Range Dielectric Spectrometer for Colloidal Suspensions: Cell Design, Calibration, and Validation. *J. Colloid Interface Sci.* **2003**, *257*, 65−76.
(39) Butzlaff, M.; Weigel, A.; Ponimaskin, E.; Zeug, A. ESIP: A Novel Solution-Based Sectioned Image Property Approach for Microscope Calibration. *PLoS One* **2015**, *10*, No. e0134980.
(40) Wilson, T. Resolution and Optical Sectioning in the Confocal Microscope. *J. Microsc.* **2011**, *244*, 113−121.
(41) Fagan, J. A.; Sides, P. J.; Prieve, D. C. Evidence of Multiple Electrohydrodynamic Forces Acting on a Colloidal Particle near an Electrode Due to an Alternating Current Electric Field. *Langmuir* **2005**, *21*, 1784−1794.
(42) Squires, T. M.; Bazant, M. Z. Induced-Charge Electro-Osmosis. *J. Fluid Mech.* **2004**, *509*, 217−252.
(43) Fagan, J. A.; Sides, P. J.; Prieve, D. C. Mechanism of Rectified Lateral Motion of Particles near Electrodes in Alternating Electric Fields below 1 KHz. *Langmuir* **2006**, *22*, 9846−9852.
(44) Miyake, T.; Rolandi, M. Grotthuss Mechanisms: From Proton Transport in Proton Wires to Bioprotonic Devices. *J. Phys.: Condens. Matter* **2015**, *28*, 023001.
(45) Feick, J. D.; Chukwumah, N.; Noel, A. E.; Velegol, D. Altering Surface Charge Nonuniformity on Individual Colloidal Particles. *Langmuir* **2004**, *20*, 3090−3095.
(46) Yake, A. M.; Snyder, C. E.; Velegol, D. Site-Specific Functionalization on Individual Colloids: Size Control, Stability, and Multilayers. *Langmuir* **2007**, *23*, 9069−9075.
(47) Bianchi, E.; Blaak, R.; Likos, C. N. Patchy Colloids: State of the Art and Perspectives. *Phys. Chem. Chem. Phys.* **2011**, *13*, 6397−6410.
(48) Boymelgreen, A.; Yossifon, G. Observing Electrokinetic Janus Particle-Channel Wall Interaction Using Microparticle Image Velocimetry. *Langmuir* **2015**, *31*, 8243−8250.
(49) Ma, F.; Wang, S.; Smith, L.; Wu, N. Two-Dimensional Assembly of Symmetric Colloidal Dimers under Electric Fields. *Adv. Funct. Mater.* **2012**, *22*, 4334−4343.
(50) Ma, F.; Wang, S.; Wu, D. T.; Wu, N. Electric-Field-Induced Assembly and Propulsion of Chiral Colloidal Clusters. *Proc. Natl. Acad. Sci. U.S.A.* **2015**, *112*, 6307−6312.

DOI: 10.1021/acs.langmuir.9b00313
Langmuir 2019, 35, 6971−6980